Two-channel model for nonequilibrium thermal transport in pump-probe experiments

R. B. Wilson,* Joseph P. Feser, Gregory T. Hohensee, and David G. Cahill

Department of Materials Science and Engineering and Materials Research Laboratory, University of Illinois, Urbana, Illinois 61801, USA

(Received 19 August 2013; revised manuscript received 23 September 2013; published 15 October 2013)

We present an analytic solution for heat flow in a multilayer two-channel system for the interpretation of time-domain thermoreflectance (TDTR) experiments where nonequilibrium effects are important. The two-channel solution is used to analyze new room temperature TDTR measurements of Al/Cu and Al/$Si_{0.99}Ge_{0.01}$ systems. Cu and $Si_{0.99}Ge_{0.01}$ are examples of materials well suited for analysis with a two-channel model because thermal excitations responsible for the vast majority of the heat capacity in these solids contribute little to their thermal conductivity. Nonequilibrium effects are found to be unimportant for the interpretation of the Al/Cu TDTR data but dramatic for the Al/$Si_{0.99}Ge_{0.01}$ TDTR data. The two-channel model predicts a significant reduction in the effective thermal conductivity of $Si_{0.99}Ge_{0.01}$ in a region within 150 nm of the Al/$Si_{0.99}Ge_{0.01}$ interface. The extra thermal resistance in this region is a result of the disparate heat flux boundary conditions for low- and high-frequency phonons in combination with weak coupling between low- and high-frequency phonons. When the experimental data are analyzed with a single-channel model, both the conductance and thermal conductivity appear to depend on pump-modulation frequency, consistent with the two-channel model's predictions. Finally, we compare the results of our diffusive two-channel model to a nonlocal description for steady-state heat flow near a boundary and show they yield nearly identical results.

DOI: 10.1103/PhysRevB.88.144305 PACS number(s): 66.70.−f, 44.05.+e, 65.40.−b

I. INTRODUCTION

The magnitude of a material's thermal conductivity and specific heat is determined by the dispersion relations, scattering rates, and occupation statistics of the material's quasiparticle excitations, e.g., electrons, phonons, and magnons. On macroscopic scales, heat flow in a material is well described by the heat diffusion equation and depends only on the magnitude of the material's heat capacity and thermal conductivity. The heat diffusion equation is a valid description of heat flow as long as all quasiparticles that store and carry heat are in local thermal equilibrium. In other words, the occupation of all thermal excitations must be well described by a single temperature on time-scales that are comparable to the rate of heating/cooling and length-scales that are comparable to the quasiparticle mean free paths. On short time and length scales, the condition of local equilibrium can break down, and microscopic knowledge concerning the system's thermal excitations is necessary to accurately predict its thermal response.

Local equilibrium often breaks down in multilayered systems due to boundaries. This is because different types of thermal excitations can have drastically different temperature and heat flux boundary conditions. For example, electrons in a metal near a metal/dielectric interface have an adiabatic boundary condition, while phonons in the metal do not; this means local thermal equilibrium cannot exist between electrons and phonons in close proximity to a metal/dielectric interface that is subjected to a heat flux.[1]

Recent studies demonstrate the ability of pump/probe methods to reveal nonequilibrium energy flow in many different types of systems.[2–7] Quantifying the strength of coupling between different types of excitations, a key goal of condensed matter physics research, is more challenging. Recent studies demonstrate that time-domain thermoreflectance (TDTR) is sensitive to the strength of coupling between thermal excitations.[3,5,7] However, the interpretation of TDTR data where nonequilibrium effects are present is not straightforward because the experimental data are typically analyzed with a solution to the heat diffusion equation that assumes the local-equilibrium condition is satisfied. To extract quantitative values for the strength of coupling between thermal excitations, a model is needed that can accurately describe nonequilibrium heat flow.

The goal of the present work is to provide a model for analyzing TDTR data that can accurately include some nonequilibrium effects. While a general treatment of nonequilibrium transport requires a solution of the Boltzmann transport equation,[8] nonequilibrium heat flow is often well-described with a diffusive two-channel model,[7] which is the approach we take here. In this approach, different excitations are divided into channels, and the heat diffusion equation is modified based on the microscopic transport properties of the carriers in each channel. Variations of the two-channel approach have been used to successfully model heat flow in systems with multiple types of heat carriers such as low-frequency ballistic phonons/high-frequency diffusive phonons,[2] electrons/phonons,[7] and magnons/phonons.[9]

The outline of the paper is as follows. In Sec. II, we present a solution for two-channel heat flow in a semi-infinite one-dimensional system. Several simple expressions are derived that are useful for quantifying the time scales, length scales, and thermal resistances associated with nonequilibrium effects. In Sec. III, we use the two-channel solution to analyze new TDTR measurements of Al/Cu and Al/$Si_{0.99}Ge_{0.01}$ systems, and compare with one-channel interpretations of the same. Interestingly, the two-channel model suggests the value of the Al/$Si_{0.99}Ge_{0.01}$ system's measured interface conductance is not intrinsic to the interface itself but is largely caused by a mismatch between the heat carriers responsible for heat flow across the Al/$Si_{0.99}Ge_{0.01}$ interface and heat flow in the $Si_{0.99}Ge_{0.01}$. This type of contribution to the interface conductance is similar to the type predicted by Majumdar and Reddy for metal/dielectric interfaces due to weak electron-phonon coupling in the metal.[1] Finally, in Sec. IV we compare

the diffusive two-channel model to a simple nonlocal model for steady-state heat flow near an interface. The two different approaches to the problem yield similar results, and both suggest the mean free path is not the only important length scale for describing nonequilibrium between carriers near an interface.

II. TWO-CHANNEL PROBLEM IN ONE DIMENSION (1D)

In a two-temperature model, thermal excitations are divided into separate channels. It is assumed that the carrier distribution in each channel can be described by a single temperature that can be distinct from the other channel's temperature.[1,10–12] Energy transfer between channels is proportional to their temperature difference. In 1D, the channel's temperatures evolve in time according to the equations

$$C_1 \frac{\partial T_1}{\partial t} = \Lambda_1 \frac{\partial^2 T_1}{\partial z^2} - g\Theta, \tag{1}$$

$$C_2 \frac{\partial T_2}{\partial t} = \Lambda_2 \frac{\partial^2 T_2}{\partial z^2} + g\Theta, \tag{2}$$

where C_1 and C_2 are the specific heats of channels 1 and 2, Λ_1 and Λ_2 are the thermal conductivities of channels 1 and 2, $\Theta = T_1 - T_2$, and g is the energy transfer coefficient between channels that depends on the strength of coupling between carriers in different channels. We assume all thermal properties are independent of temperature, i.e., that Eqs. (1) and (2) are linear. Therefore, our model will not apply when temperature excursions of either channel are large enough to invalidate this assumption.

Before solving Eqs. (1) and (2) in the frequency domain, it is useful to look at the solution for $\Theta = T_1 - T_2$ in the spatially uniform and steady state limits. These solutions are found by solving the differential equation that results from the subtraction of Eq. (2) from Eq. (1). In the spatially uniform limit, $\partial^2 T/\partial z^2 = 0$, the temperature difference between channels decays exponentially with a time constant of

$$\Gamma = (g/C_1 + g/C_2)^{-1}. \tag{3}$$

This is the thermal relaxation time of the two channels in the absence of heating. Values for relaxation times will range from tens of femtoseconds to hundreds of picoseconds, depending on the type of carriers that make up each channel. Since the time scale for pump modulation in TDTR experiments is typically greater than 50 ns, thermal resistances that result from a difference in temperature between channels will not depend on the pump-modulation frequency.

In the steady state limit, $\partial T/\partial t = 0$, the difference in temperature between the channels will exponentially decay on a length scale of

$$d = (g(1/\Lambda_1 + 1/\Lambda_2))^{-1/2}. \tag{4}$$

Any thermal resistance caused by nonequilibrium effects will be distributed across this length. Typical values at room temperature will range from nanometers to hundreds of nanometers.

The values of d and Γ are useful for determining if nonequilibrium effects in a TDTR experiment are distinguishable from other thermal parameters in the system. For example, the value Γ will often be comparable to other time scales in the problem, such as pump- or probe-pulse duration, the thermal relaxation time for a metal transducer, $(h^2C)/\Lambda$, or the time constant for heat to diffuse across an interface,[13] $(hC)/G$. Similarly, if d is much less than other important length scales in TDTR experiments such as transducer thickness, metal/sample Kapitza length, thermal penetration depth, and laser spot size, then the nonequilibrium resistance may not be distinguishable from other thermal resistances.

Because d is often small compared to other important length scales, the most common result of using a single channel model to describe a two-channel system is to combine into a single effective value the thermal conductance associated with the nonequilibrium between channels and the interfacial thermal conductance. We follow Majumdar and Reddy's derivation of an effective conductance that includes nonequilibrium effects for an electron-phonon system[1] and consider the steady-state solutions to Eqs. (1) and (2); however, we do not initially require an adiabatic boundary condition on one of the channels. We assume each channel has an interface conductance, G_1 and G_2, that determines heat flow into that channel at the boundary,

$$q_i = G_i(T_0 - T_i), \tag{5}$$

where T_0 is the temperature of the single-temperature layer at the boundary and $i = 1,2$. The temperatures in each channel are then

$$T_1 = \gamma a \frac{gd^2}{\Lambda_1} e^{-z/d} + az + T_b, \tag{6}$$

$$T_2 = \gamma a \left(\frac{gd^2}{\Lambda_1} - 1\right) e^{-z/d} + az + T_b, \tag{7}$$

$$\gamma = \frac{1}{dg}\left(\frac{\Lambda_2}{G_2} - \frac{\Lambda_1}{G_1}\right)\left(\frac{1}{G_1} + \frac{d}{\Lambda_1} + \frac{1}{G_2} + \frac{d}{\Lambda_2}\right)^{-1}, \tag{8}$$

where a and T_b are constants that depend on T_0. Assuming equilibrium between channel temperatures is equivalent to assuming that the boundary temperature of both channels is T_b $(d = 0)$. The effective conductance in this case is

$$G_{\text{eff}} = \frac{q_1 + q_2}{T_0 - T_b} = \frac{-(\Lambda_1 + \Lambda_2)}{\gamma dg(1/G_2 + d/\Lambda_2) - \Lambda_2/G_2} = \left(\frac{1}{G_{\text{NE}}} + \frac{1}{G_1 + G_2}\right)^{-1}. \tag{9}$$

where G_{NE} is defined as the nonequilibrium conductance.

In many systems, one channel's interface conductance is much lower than the others. For example, at a semiconductor boundary with a metal, the interface conductance for low-frequency phonons is small compared to high-frequency phonons because of their relative number of states.[14] (Heat flux across a plane due to a specific phonon is proportional to the difference in temperature on either side of the plane, the mode's group velocity, and the mode's number density.) In these situations, the limiting case of an adiabatic boundary condition for one channel, $G_1 \approx 0$, is useful for quickly determining whether nonequilibrium resistances will be significant in the system. For the adiabatic case, the effective interface resistance simplifies to the sum of interfacial and nonequilibrium resistances,

$$\frac{1}{G_{\text{eff}}} = \frac{1}{G_2} + \frac{\Lambda_1 d}{\Lambda_2(\Lambda_1 + \Lambda_2)} = \frac{1}{G_2} + \frac{1}{G_{\text{NE}}}. \tag{10}$$

In the limit that $\Lambda_2 \gg \Lambda_1$, Eq. (10) predicts a nonequilibrium conductance of $G_{NE} = \Lambda_2^2/(\Lambda_1 d)$, much larger than most interfacial thermal conductance values. A large conductance means a small resistance, and resistances combine additively. Therefore, in situations where a high-thermal conductivity channel has a large interface conductance, nonequilibrium effects can be safely ignored. In the opposite limit, $\Lambda_2 \ll \Lambda_1$, Eq. (9) predicts a nonequilibrium conductance of Λ_2/d, a value that is sometimes comparable to measured interfacial conductance values.[14,15] For example, consider Au at room temperature with phonons as channel 2 and electrons as channel 1. Using a value of 3 W m^{-1} K^{-1} for the lattice thermal conductivity of Au (extrapolated form measurements below 100 K[16]) and a coupling strength of 2.5×10^{16} W m^{-3} K^{-1} between electrons and phonons in Au[7], the above equations yield $d \approx 10$ nm and $G_{NE} \approx 300$ MW m^{-2} K^{-1}, which is a conductance comparable to observed values for phonon-phonon interface conductance.[14,15] A similar analysis for Ag and Cu, again using values for the lattice thermal conductivity extrapolated from measurements below 100 K (Refs. 17 and 18) and literature values for the electron-phonon coupling strength,[7,19] yields 350 MW m^{-2} K^{-1} and 750 MW m^{-2} K^{-1}, respectively. In most other metals, the nonequilibrium conductance will be much higher because of stronger electron-phonon coupling than is present in the group 1B metals.[19] We conclude that electron-phonon coupling is rarely a significant source of thermal resistance compared to phonon-phonon interfacial thermal conductance values.

In semiconductors, we can estimate the expected coupling constant between the low-frequency phonons, which carry significant amounts of heat, and high-frequency phonons, which form the majority of the heat capacity, by assuming the minimum possible thermal relaxation time, Γ, is equal to the scattering times of low-frequency phonons (<3 THz). Low-frequency phonons in semiconductors will nearly always have lifetimes greater than 10 ps; for example, estimates of the lifetimes of 3 THz phonons in Si range from 50 to 180 ps.[20,21] We estimate the heat capacity of low-frequency phonons to be on the order of 10^4 J m^{-3} K^{-1} and the thermal conductivity of the thermal reservoir as between 10 and 30 W m^{-1} K^{-1}. Then, using Eq. (3), a reasonable estimate for the coupling constant between low- and high- frequency phonons is on the order of 10^{15} W m^{-3} K^{-1}, and Eq. (10) predicts a nonequilibrium conductance on the order of 100 MW m^{-2} K^{-1}. This is comparable to typical metal/semiconductor interface conductance values observed in TDTR experiments[15] and suggests nonequilibrium effects are an important contribution to the observed interface conductance values in metal/semiconductor systems.

In the frequency-domain, Eqs. (1) and (2) become

$$\frac{\partial^2 T_1}{\partial z^2} = \alpha_1 T_1 - \frac{g}{\Lambda_1} T_2, \tag{11}$$

$$\frac{\partial^2 T_2}{\partial z^2} = \alpha_2 T_2 - \frac{g}{\Lambda_2} T_1, \tag{12}$$

where $\alpha_1 = 1/\Lambda_1(i\omega C_1 + g)$ and $\alpha_2 = 1/\Lambda_2(i\omega C_2 + g)$. The differential equations in Eqs. (11) and (12) can be solved as an algebraic eigenvalue problem by assuming a solution of the form $T = ve^{\lambda z}$. The general solution to Eqs. (11) and (12) in matrix form is

$$\begin{bmatrix} T_1 \\ T_2 \end{bmatrix} = [X] \begin{bmatrix} B_1^- e^{-\lambda_1 z} + B_1^+ e^{\lambda_1 z} \\ B_2^- e^{-\lambda_2 z} + B_2^+ e^{\lambda_2 z} \end{bmatrix}, \tag{13}$$

where λ^2 are the eigenvalues of the characteristic matrix

$$\begin{bmatrix} \alpha_1 & -g/\Lambda_1 \\ -g/\Lambda_2 & \alpha_2 \end{bmatrix}$$

and $[X]$ is the associated eigenvector matrix

$$[X] = \begin{bmatrix} v_1 & v_2 \\ u_1 & u_2 \end{bmatrix}. \tag{14}$$

For the case of a semi-infinite solid $B^+ = 0$, because there is no reflected thermal wave and therefore no wave propagating toward the surface. Applying a heat flux boundary condition $q = -\Lambda(dT/dz)_{z=0}$ to each channel gives the solution

$$\begin{bmatrix} B_1^- \\ B_2^- \end{bmatrix} = [Y]^{-1} \begin{bmatrix} q_1 \\ q_2 \end{bmatrix}, \tag{15}$$

where

$$[Y] = \begin{bmatrix} \Lambda_1 & 0 \\ 0 & \Lambda_2 \end{bmatrix} [X] \begin{bmatrix} \lambda_1 & 0 \\ 0 & \lambda_2 \end{bmatrix}. \tag{16}$$

Further details for generalizing Eqs. (11)–(16) for a radially symmetric multilayer problem and integrating the two-channel solution with the standard analytical techniques for TDTR analysis are given in Appendix A.

Example calculations using Eqs. (11)–(16) are shown in Fig. 1 for Cu and $Si_{0.99}Ge_{0.01}$. For Cu, the phonons and electrons are divided into separate channels, and oscillatory heating at the surface is restricted to phonons only. The Cu thermal properties used are $\Lambda_1 = 392$ W m^{-1} K^{-1}, $\Lambda_2 = 7$ W m^{-1} K^{-1}, $C_1 = 3 \times 10^4$ J m^{-3} K^{-1}, $C_2 = 3.42 \times 10^6$ J m^{-3} K^{-1}, and $g = 7.5 \times 10^{16}$ W m^{-3} K^{-1}. The out-of-phase temperature oscillations of Cu shows no significant deviation compared to a one-channel model calculation with bulk properties at frequencies below 20 MHz [Fig. 1(b)]. The out-of-phase signal in a TDTR measurement is dominated by the imaginary part of the frequency response at the pump-modulation frequency.[22] Therefore, any impact from the difference in temperature between channels in Cu will only appear in the in-phase temperature response of a TDTR experiment, which includes high-frequency components associated with pulse-decay timescales.[22]

For $Si_{0.99}Ge_{0.01}$, we divide the low-frequency phonons (<3 THz) and high-frequency phonons into separate channels with an adiabatic surface boundary condition imposed on the low-frequency phonons. The thermal properties of the channels in the $Si_{0.99}Ge_{0.01}$ layer are $\Lambda_1 = 30$ W m^{-1} K^{-1}, $\Lambda_2 = 12$ W m^{-1} K^{-1}, $C_1 = 3 \times 10^4$ J m^{-3} K^{-1}, $C_2 = 1.62 \times 10^6$ J m^{-3} K^{-1}, and $g = 4 \times 10^{14}$ W m^{-3} K^{-1}. The division of the total thermal conductivity between channels 1 and 2 and the coupling strength, g, are based on the experimental results presented in Sec. III. The division of heat capacity between channels is calculated from the Si density of states.[23] The division frequency of 3 THz was chosen so that only phonon modes with linear dispersion and low-heat capacity are included in the low-frequency channel.[23] Unlike Cu, both the out-of-phase and

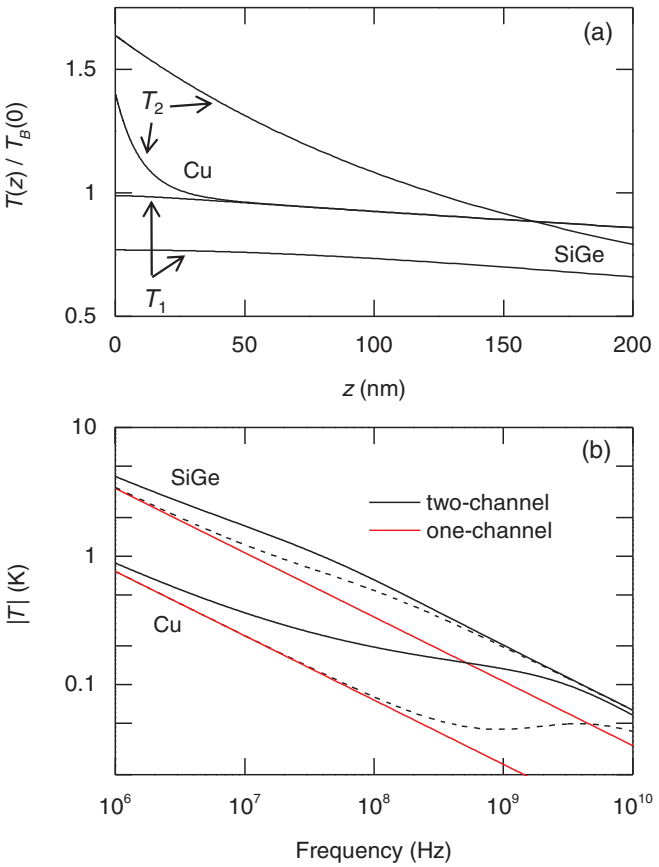

FIG. 1. (Color online) Calculated frequency response of 1D semi-infinite two-channel Cu and $Si_{0.99}Ge_{0.01}$ layers. For Cu, T_1 and T_2 are the temperature of the electrons and phonons, while in $Si_{0.99}Ge_{0.01}$, T_1 and T_2 describe the low- and high-frequency phonons. Thermal properties of both systems are described in the text. (a) Amplitude of temperature oscillations for each channel as a function of depth at a heating frequency of 20 MHz. The temperature rise of each channel is normalized with the prediction for surface temperature from a one channel model with bulk properties, $T_B(0)$. (b) Surface temperature of channel 2 as a function of heating frequency. Solid lines are the in-phase temperature and dashed lines are the out-of-phase temperature. A one-channel model predicts no difference in the in-phase and out-of-phase temperature response.

the in-phase surface temperature oscillations of $Si_{0.99}Ge_{0.01}$ [Fig. 1(b)] display a significant deviation from the single-channel model's prediction at all frequencies above 1 MHz. Thus, nonequilibrium between channels can be expected to influence TDTR experiments through both the in-phase and out-of-phase signals of a TDTR experiment.

The frequency dependence of the thermal response shown in Fig. 1 will be qualitatively similar to any two-channel system where the majority of heat is carried by thermal excitations with very little heat capacity, such as other metals[7] (electrons), semiconductor alloys[3] (low-frequency phonons), or spin ladders[24] (magnons). In 1D, solids with homogenous thermal properties will have in-phase and out-of-phase surface temperature oscillations that are equal in magnitude. The difference in amplitude between the in-phase and out-of-phase temperature oscillations for the two-channel systems in Fig. 1 indicates that the thermal properties of the system are not homogenous in the region of the system that is transporting heat, and that a single effective thermal conductivity cannot describe the system's transient thermal response.

III. ANALYSIS OF EXPERIMENTAL TDTR DATA WITH A TWO-CHANNEL MODEL

Example calculations of TDTR data for a two-channel multilayer system are shown in Fig. 2. The system consists of an 80-nm single-channel Al transducer on top of a semi-infinite two-channel $Si_{0.99}Ge_{0.01}$ layer. Low-frequency $Si_{0.99}Ge_{0.01}$

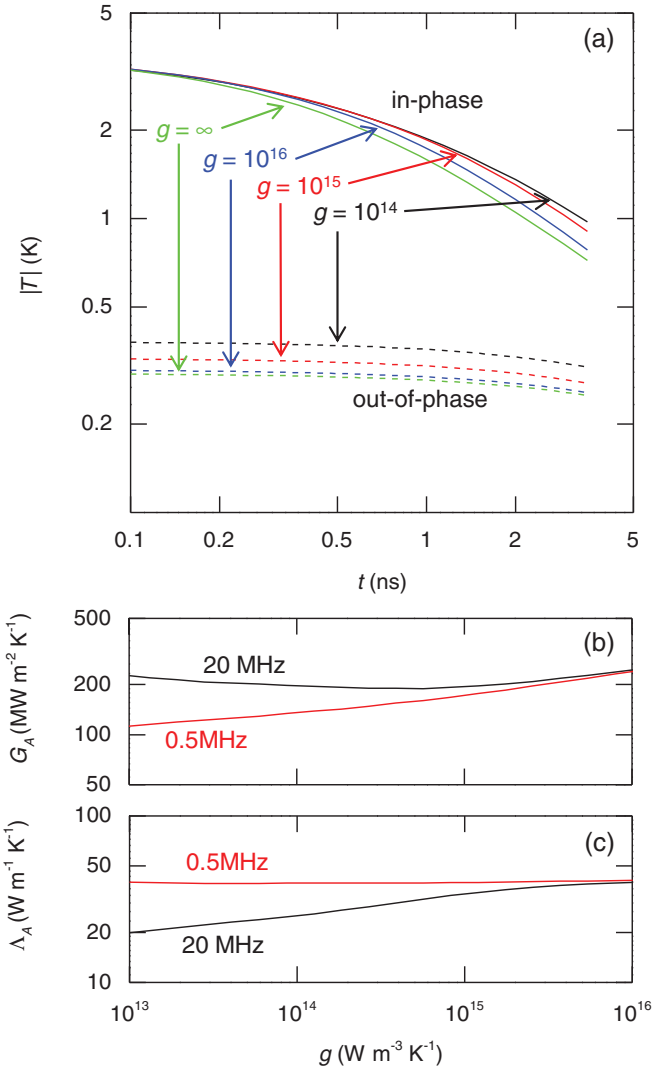

FIG. 2. (Color online) (a) Calculated dependence of TDTR data on coupling strength, g, at fixed modulation frequency of 20 MHz and $1/e^2$ laser spot size of 10 μm for an 80 nm Al/$Si_{0.99}Ge_{0.01}$ two-channel system. The units of g are W m^{-3} K^{-1}. The apparent interface conductance and thermal conductivity are defined as the values that result from analyzing the two-channel data with a single-channel model. The apparent interface conductance is primarily determined by the time decay of the in-phase signal, while the apparent thermal conductivity is primarily determined by the magnitude of the out-of-phase signal. (b) The apparent interface conductance G_A versus coupling strength. (c) The apparent thermal conductivity Λ_A versus coupling strength.

phonons (<3 THz) form channel 1, while high-frequency phonons make up channel 2. Thermal properties of the channels in the $Si_{0.99}Ge_{0.01}$ layer are the same as those described in Sec. II for Fig. 1. The interface conductance values between the Al and $Si_{0.99}Ge_{0.01}$ channels are $G_1 = 30$ MW m^{-2} K^{-1} and $G_2 = 320$ MW m^{-2} K^{-1}. The total conductance was chosen based on the lattice dynamics calculation in Ref. 25 with $a = 0.2$ nm, $K' = 2.5$, $M' = 1$, and an Al Debye temperature of 400 K. The conductance for the low-frequency phonons, G_1, was set to the phonon radiation limit value for phonons less than 3 THz (Ref. 15). Setting G_1 to a lower value will increase the thermal resistance due to nonequilibrium effects.

We define an apparent thermal conductivity, Λ_A, and apparent interface conductance, G_A, as the values extracted by fitting TDTR signals using a one-channel model.[22] We can calculate apparent thermal conductivity and conductance values for a hypothetical two-channel system by fitting TDTR signals generated using the two-channel model with a single-channel model. The value of Λ_A depends primarily on the magnitude out-of-phase TDTR signal, while G_A depends primarily on the decay rate of the in-phase TDTR signal with the delay time between pump and probe pulses. Figures 2(b) and 2(c) show calculated Λ_A and G_A values as a function of coupling strength for the two-channel Al/$Si_{0.99}Ge_{0.01}$ system described above. The pump-modulation frequency dependence observed in the Λ_A and G_A values is a result of assuming a homogenous $Si_{0.99}Ge_{0.01}$ thermal conductivity, thereby ignoring the reduced ability of the $Si_{0.99}Ge_{0.01}$ to transport heat within a length d of the interface. The thermal resistance caused by the two channels having different temperatures is independent of the pump-modulation frequency; it appears even at steady state [see Eq. (9)]. However, the sensitivity of the surface temperature to the thermal properties of the region near the interface is a function of pump-modulation frequency. At low pump-modulation frequencies (<1 MHz), nonequilibrium thermal resistance manifests as a significant reduction in G_A for the Al/$Si_{0.99}Ge_{0.01}$ system. At higher pump-modulation frequencies (>1 MHz), the out-of-phase temperature is more sensitive to the thermal properties of the region near the Al/$Si_{0.99}Ge_{0.01}$ interface, thereby causing the nonequilibrium resistance to also appear as a reduction in Λ_A.

Figure 3 shows Λ_A and G_A derived from room temperature TDTR measurements of Al/Cu and Al/$Si_{0.99}Ge_{0.01}$ samples, along with predictions of the two-channel model. The pump and probe $1/e^2$ spot sizes for the TDTR measurement were 10.3 μm. The Ge content of the dilute Si alloy was determined to be 0.9% by Rutherford backscattering spectroscopy. The 80-nm Al metal films were deposited on the $Si_{0.99}Ge_{0.01}$ and Cu substrates using dc magnetron sputtering in a high vacuum chamber. The substrates were temporarily heated to ~600 °C under high vacuum and allowed to cool to room temperature prior to Al deposition in order to provide a cleaner interface.

For the two-channel analysis of Cu, electrons are grouped into channel 1, phonons into channel 2, and the thermal properties for each channel are the same as defined in Sec. II for Fig. 1. We expect an adiabatic condition between the Al and Cu electrons as a result of the Cu native oxide and set $G_1 = 0$. The phonon-phonon interface conductance is treated as a fitting parameter and is adjusted so G_A derived from the two-channel model matches G_A derived from the experimental

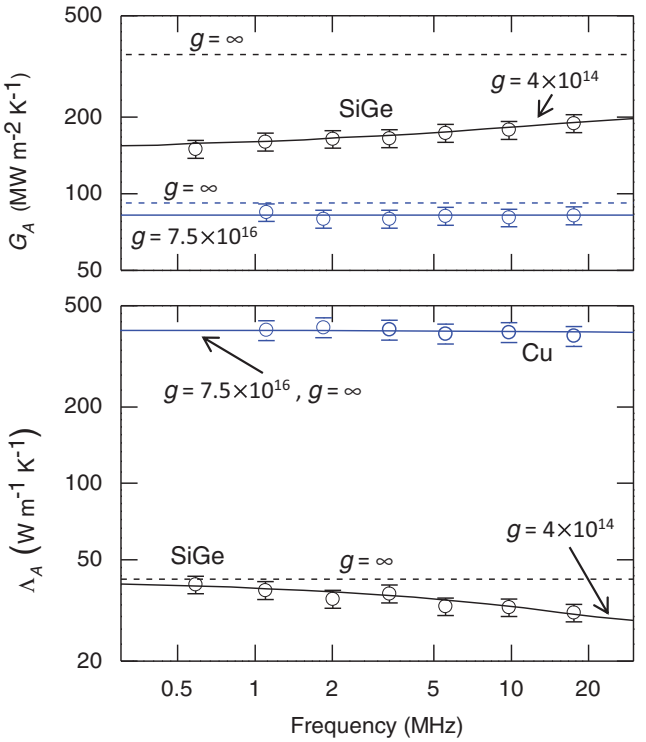

FIG. 3. (Color online) Apparent thermal conductivity and interface conductance from TDTR measurements of Al/Cu and Al/$Si_{0.99}Ge_{0.01}$ systems as a function of pump-modulation frequency. Lines indicate the results of fitting TDTR signals generated by the two-channel model with a single-channel model. The units of g are W m^{-3} K^{-1}.

data. A value of $G_2 = 92$ MW m^{-2} K^{-1} results in good agreement. This value is much less than the 4 GW m^{-2} K^{-1} conductance previously observed for clean Al/Cu interfaces,[26] confirming our expectation of an adiabatic boundary condition on electrons. The nonequilibrium conductance calculated from Eq. (9) is 750 MW m^{-2} K^{-1}, much larger than the phonon-phonon conductance. The length scale of the nonequilibrium calculated from Eq. (4) is only 10 nm, much less than the thermal penetration depth in Cu (>2 μm). For these reasons, nonequilibrium effects are indistinguishable from the phonon-phonon conductance, and the two-channel model is unnecessary for interpreting the results.

For $Si_{0.99}Ge_{0.01}$, the two-channel thermal properties are set to the previously described values, and g, Λ_2, and $\Lambda_1 + \Lambda_2$ are adjusted until Λ_A and G_A calculated from the two-channel model match the experimental values. Values of $g = 4 \times 10^{14}$ W m^{-3} K^{-1}, $\Lambda_2 = 12$ W m^{-1} K^{-1}, and $\Lambda_1 + \Lambda_2 = 42$ W m^{-1} K^{-1} result in excellent agreement. A coupling constant on the order of 10^{14} W m^{-3} K^{-1} is expected based on the scattering times of low-frequency phonons in Si (Refs. 20 and 21). The total thermal conductivity of 42 ± 4 W m^{-1} K^{-1} we find for $Si_{0.991}Ge_{0.009}$ is higher than the previously reported value of 30 W m^{-1} K^{-1} for a 1-μm-thick thin film of $Si_{0.99}Ge_{0.01}$ (Ref. 27). While thin films often have reduced thermal conductivity values compared to the bulk, the prior TDTR study did not consider the possibility of a suppressed value due to the 10 MHz pump-modulation frequency used. The similarity between the value we obtain at 10 MHz of

32 W m^{-1} K^{-1} and the prior result of 30 W m^{-1} K^{-1} suggest that the effect of using a high pump-modulation frequency may not have been negligible. However, because the 800-nm thermal penetration depth in $Si_{0.99}Ge_{0.01}$ at 10 MHz is comparable to the 1-μm film thickness, the error is likely small.

We observe frequency dependence in the apparent interface conductance of the Al/$Si_{0.99}Ge_{0.01}$ system (Fig. 3), a phenomena that has not been previously reported. The two-channel model suggests the frequency dependence is a result of (1) the in-phase decay of the Al/$Si_{0.99}Ge_{0.01}$ system being sensitive to both the interface conductance and the thermal effusivity within a distance d of the interface; and (2) the magnitude of the out-of-phase signal being sensitive to the thermal effusivity of the SiGe within d of the interface. Previous reports of TDTR frequency-dependent Λ_A have been for low thermal conductivity, high concentration alloys, where the in-phase decay rate is primarily determined by the small effusivity of the sample and therefore were not sensitive to this type of effect. Prior TDTR measurements of high thermal conductivity solids, such as Si, have revealed no frequency dependence in Λ_A or G_A. This is consistent with the two-channel model, since high diffusivity solids will have thermal penetration depths much larger than d at the pump-modulation frequencies accessible in TDTR experiments (<20 MHz). Frequency-domain thermoreflectance (FDTR) can access higher pump-modulation frequencies but cannot independently determine Λ_A and G_A at a single frequency; therefore, all FDTR studies to date have assumed that G_A is a constant value.[6,28]

Because TDTR is sensitive to thermal effusivity, it derives its sensitivity to the thermal parameters in the two-channel model indirectly based on how they affect $T_2(z)$, the temperature profile of the high heat capacity channel. As a result, Λ_A and G_A derived from the two-channel model do not depend on g, Λ_2, and G_1 independently of each other, and we cannot uniquely determine all parameters from the experimental data. The low-frequency TDTR measurements yield approximate values for $\Lambda_1 + \Lambda_2$ and G_{eff}. The frequency dependence of Λ_A and G_A provides information about the thermal resistance due to nonequilibrium between channels, i.e., it provides approximate values for $1/G_{NE}$ and d. Any combination of parameters that results in $\Lambda_1 + \Lambda_2 \approx 42$ W m^{-1} K^{-1}, $d \approx 150$ nm, and $G_{NE} \approx 200$ MW m^{-2} K^{-1} will yield similar results.

Although the nonequilibrium in surface temperatures is due to a difference in temperature between heat carriers, the effect can be closely approximated using a single channel model by inserting a low thermal conductivity film of thickness d at the surface of the bulk solid. The thermal conductivity of the layer can be calculated by adding the a thermal resistance of $1/G_{NE}$ to the intrinsic thermal resistance of the film, $d/(\Lambda_1 + \Lambda_2)$. A single-channel bilayer model with a thin film of thickness $d = 150$ nm, heat capacity of 1.65 J cm^{-3} K^{-1}, and thermal conductivity of $\Lambda_{tf} = d(d/(\Lambda_1 + \Lambda_2) + 1/G_{NE})^{-1} =$ 17 W m^{-1} K^{-1}, on top of a semi-infinite $Si_{0.99}Ge_{0.01}$ layer with bulk properties, yields nearly equivalent results as the two-channel model. Similarly, for the Cu system, a single-channel model for a 10-nm-thick film with a thermal conductivity of 7 W m^{-1} K^{-1} on top of a semi-infinite Cu layer with bulk properties yields identical results to the two-channel model. The reason this thin-film approximation works is it predicts a temperature profile similar to the two-channel model's prediction for the high heat capacity channel $T_2(z)$.

IV. DIFFUSIVE TWO-CHANNEL MODEL VERSUS BALLISTIC/DIFFUSIVE TWO-CHANNEL MODEL

A relevant question when applying the diffusive two-channel model to $Si_{0.99}Ge_{0.01}$ is whether splitting up high- and low-frequency phonons into two *diffusive* channels is justified; most of the low-frequency phonons have mean free paths larger than d [Eq. (4)]. In this section, we address this issue and discuss how our two-channel, two-temperature model relates to prior explanations of frequency-dependent thermal conductivity in TDTR measurements.[3,29]

Previous observations of frequency-dependent thermal conductivity measured by TDTR, as well as the similar technique FDTR, have been interpreted phenomenologically as a mean free path effect that results from nonlocal heat flow.[3,6] In this interpretation, phonons with mean free paths larger than the thermal penetration depth do not contribute to the experimentally measured thermal conductivity. The mean free path explanation is similar to the multiple-channel picture described here but is not identical. In both interpretations, long lifetime phonons become decoupled from the thermal reservoir and do not contribute to the measured thermal conductivity when the thermal penetration depth is less than a given length scale (mean free path or d). Aside from the difference in length scales, another important difference is that in the diffusive two-channel model, it is the heat flux boundary conditions at the interface, rather than the nonlocal nature of the heat flow, that is solely responsible for the decoupling of high- and low-frequency phonons.[8]

The impact of an interface on a nonlocal description of heat flow has not been discussed in the prior TDTR and FDTR studies that have posited that nonlocal heat flow is the source of observed deviations from bulklike behavior.[3,5,6] However, the temperature profile of a solid near interfaces has a strong curvature; therefore, nonlocal effects are likely to be important near boundaries. To better understand the role of interfaces in nonlocal transport, and to better understand the relationship between the diffusive two-channel model and nonlocal theory, we consider a simple model for steady-state ballistic heat flow in 1D. Heat flux across a plane, q, in a homogenous solid due to one type of thermal excitation is equal to the product of the excitation's volumetric number density, n, the excitation's group velocity, v, and the difference in energy between excitations traveling in the positive and negative directions, ΔE, i.e., $q = nv\Delta E/2$. We assume the thermal energy of the excitation is determined by the temperature at the position at which it was last scattered. For small energy differences, $\Delta E = dE/dT(\Delta T)$ and $q = Cv\Delta T/2$, where ΔT is the average difference in temperature of the positions where excitations crossing the plane last scattered. If the temperature profile near the plane can be approximated with the local temperature gradient, i.e., $\Delta T = -2\ell\, dT/dz$, then heat flow is diffusive and $q = Cv\ell(-dT/dz)$. When the temperature profile near the plane cannot be approximated by the local temperature gradient, meaning the temperature profile is not a linear function of position on the length scale

of the mean free path, the ballistic heat flux, q_B, is

$$q_B = \frac{Cv}{2}(\bar{T}(-\infty \to z) - \bar{T}(z \to \infty)), \quad (17)$$

$$\bar{T}(-\infty \to z) = \int_{-\infty}^{z} T(x)/\ell \exp(-(z-x)/\ell)dx, \quad (18)$$

$$\bar{T}(z \to \infty) = \int_{z}^{\infty} T(x)/\ell \exp(-(x-z)/\ell)dx. \quad (19)$$

To include the effect of an interface with another layer at $z = 0$, $\bar{T}(-\infty \to z)$ needs to be redefined to allow excitations to transmit or reflect at the boundary

$$\bar{T}(-\infty \to z) = \int_{0}^{z} T(x)/\ell \exp(-(z-x)/\ell)dx + \int_{0}^{\infty} (RT(x) + (1-R)T_0)/\ell \times \exp(-(x+z)/\ell)dx, \quad (20)$$

where R is the probability of reflection, and T_0 is the temperature of the other layer, which we assume is constant. Figure 4 shows how a boundary with a constant temperature layer affects the steady-state heat flux for different mean free path thermal excitations. The long mean free path phonons have a lower heat flux near the interface. This is analogous to the low-frequency phonons in the diffusive two-channel model having a small interface conductance.

To compare the predictions of this simple description of ballistic heat flow to the results of the diffusive two-channel model, we consider a two-channel ballistic/diffusive model. Channel 1 is made up of ballistic phonons with a small heat capacity and constant inelastic scattering time, τ, and whose contribution to the heat current is given by Eqs. (17)–(20). This channel is analogous to the low-frequency phonon channel in the diffusive model. Channel 2 is made up of diffusive phonons with a large heat capacity whose contribution to the heat current is given by Fourier's law. This channel is analogous to the high-frequency phonon channel in the diffusive model. In the ballistic/diffusive model there is only one temperature: the temperature of the thermal reservoir. This reservoir can transport energy through diffusion and by radiating and absorbing low-frequency phonons. This type of model has previously been used to interpret quasiballistic transport[21] and is justified physically because most three-phonon scattering events for low-frequency phonons include two high-frequency phonons. The mean free path of the ballistic phonons in the z direction is ℓ. The total heat flux will be given by the solution to the integro-differential equation, $q = -\Lambda_2 dT/dz + q_B$. A temperature profile of the form $T(z) = H \times \exp(-z/\delta) + az$ satisfies this equation. The surface temperature, H, and temperature decay length, δ, can be found by requiring the total heat flow from diffusive and ballistic channels to be independent of z and by rejecting nonphysical solutions:

$$\delta = \left(\frac{\Lambda_2}{\Lambda_1 + \Lambda_2}\right)^{1/2} \ell. \quad (21)$$

This is identical to the decay length predicted by the diffusive two-channel model, d, if $\Gamma = \tau$, where d and Γ are defined in Eqs. (3) and (4).

In the limit that the low-frequency phonons are adiabatic, $R = 1$ and $\Gamma = \tau$, the nonlocal and diffusive models produce identical results, i.e., $H = T_2(0)$, where T_2 is defined in Eq. (7). A decrease in R increases the quantity of heat carried in the ballistic channel and reduces the surface temperature of the thermal reservoir, H. Similarly, for the diffusive two-channel model, an increase in G_1 increases the quantity of heat carried in the low-frequency phonon channel and reduces the surface temperature of the high-frequency phonon channel, $T_2(0)$. However, away from the adiabatic limit, the two models do not predict identical results; the ballistic/diffusive model predicts a lower value for the surface temperature than the diffusive model. In the ballistic/diffusive model, the heat flow between layers, within a length δ of the interface due to low-frequency phonons, is related to $T_0 - \bar{T}(0 \to \infty)$. In the diffusive two-channel model, the heat flow between layers, due to low-frequency phonons, is proportional to $T_0 - T_1$, and the heat flow in the solid, due to low-frequency phonons, is equal to $-\Lambda_1 \frac{dT_1}{dz}$. Despite this difference, the results of both models are similar because both require high-frequency phonons to carry the majority of heat diffusively near an interface, and both models have a parameter (G_1 and R) that adjusts how much heat is carried near the interface by the low-frequency channel.

A key insight from the comparison of the two models is that when an interface is responsible for decoupling low- and high-frequency phonons, the important length-scale for deviation from Fourier's law is δ or d. This means that the low-frequency phonon channel having mean free paths longer than d does not invalidate the use of the diffusive two-channel TDTR model for experimental analysis. Qualitative consideration of the ballistic/diffusive model in steady-state reveals why the ballistic mean free path is not the only important length scale. Away from the interface, the temperature gradient is linear, and both

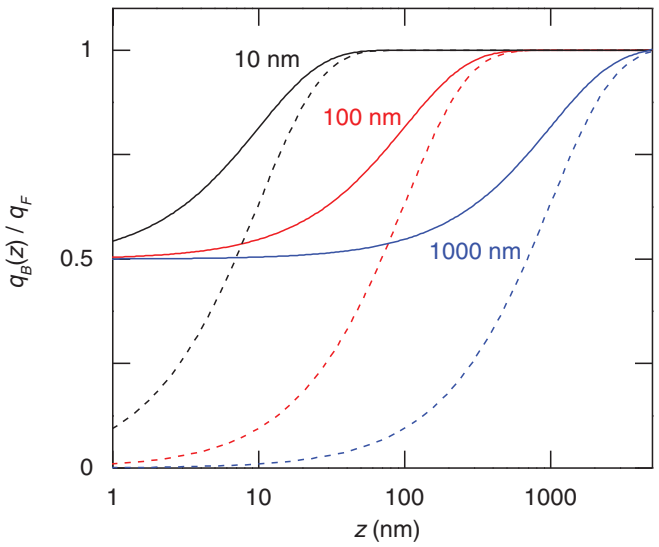

FIG. 4. (Color online) The ratio of heat flow for ballistic phonons, q_B, to the value predicted by Fourier's law, $q_F = Cv_z\ell_z$, for steady-state conditions and a boundary that transmits and reflects phonons at $z = 0$. The curves were calculated with Eq. (17) for a linear temperature gradient at $z > 0$. The temperature is assumed to be continuous at $z = 0$ and constant at $z < 0$. Solid lines represent the radiation limit ($R = 0$), while dashed lines represent the adiabatic limit ($R = 1$).

the diffusive and ballistic channels carry significant heat. For steady-state heat flow, q is independent of position; therefore, a reduced ability to transport heat ballistically near the interface results in an increase in the amount of heat that is carried diffusively near the interface. The quantity of heat the thermal reservoir carries diffusively depends on Λ_2. Therefore, the length scale describing the deviation from Fourier's law should depend on both the ballistic mean free path and thermal conductivity of the thermal reservoir, as Eq. (21) predicts. A second important insight from both models is that elastic and inelastic scattering events do not have equivalent effects; only inelastic scattering is responsible for energy transfer between channels. The importance of distinguishing between elastic and inelastic scattering has been previously described in Ref. 29.

V. CONCLUSION

In summary, we presented a two-channel model for the analysis of TDTR experiments for use in systems where nonequilibrium heat flow is important. The key insight from the two-channel model is that weak coupling between thermal excitations, combined with different heat flux boundary conditions, can result in a significant reduction of a material's ability to transport heat near an interface. We have shown that the two-channel model can explain an apparent frequency dependence of the TDTR-derived thermal conductivity and interface conductance of $Si_{0.99}Ge_{0.01}$. Finally, we explored the role an interface plays in ballistic heat flow and demonstrated that a simple ballistic/diffusive model of heat flow near an interface yields nearly identical results as the diffusive two-channel model.

ACKNOWLEDGMENTS

The experimental work and data analysis was supported by the US Department of Energy Office of Basic Energy Sciences under Grant No. DE-FG02-07ER46459. It was carried out in the Laser and Spectroscopy Laboratory of the Materials Research Laboratory at the University of Illinois Urbana-Champaign. The development of the two-channel model algorithm was supported by the Army Research Office under Grant No. W911NF-11-10526. R. B. Wilson thanks the Department of Defense for the NDSEG fellowship that supported him during this work.

APPENDIX A: TDTR ANALYSIS WITH TWO-CHANNEL SOLUTION

To interpret TDTR experiments, a thermal model that predicts the surface temperature of a radially symmetric multilayered system in response to surface heating is needed.[22,28,30] In the frequency domain, the intensity-averaged surface temperature response is[22]

$$\Delta T(\omega) = 2\pi A \int_0^\infty G(k,\omega) \exp\left(-\pi^2 k^2 \left(\omega_1^2 + \omega_2^2\right)/2\right) k dk, \tag{A1}$$

where A is the amplitude of heat absorbed by the sample surface, ω_1 and ω_2 are the pump and probe spot sizes, and $G(k,\omega)$ is equal to $T_s(k,\omega)/q_s(k,\omega)$, where T_s and q_s are the temperature and heat flux at the system's surface. To incorporate two-channel heat flow into a multilayered thermal model for TDTR analysis, it is necessary to modify the computation of $G(k,\omega)$.

The solutions generated for a 1D two-channel system are easily generalized to a three-dimensional (3D) cylindrically symmetric layer. In cylindrical coordinates, Eqs. (1) and (2) become

$$C_1 \frac{\partial T_1}{\partial t} = \Lambda_1 \left(\frac{\eta_1}{r} \frac{\partial}{\partial r} \left(\frac{\partial T_1}{\partial r} \right) + \frac{\partial^2 T_1}{\partial z^2} \right) + g(T_2 - T_1), \tag{A2}$$

$$C_2 \frac{\partial T_2}{\partial t} = \Lambda_2 \left(\frac{\eta_2}{r} \frac{\partial}{\partial r} \left(\frac{\partial T_2}{\partial r} \right) + \frac{\partial^2 T_2}{\partial z^2} \right) + g(T_1 - T_2), \tag{A3}$$

where η_1 and η_2 are the ratio of the thermal conductivities in the radial and z directions of channel 1 and 2. Taking the Hankel and Fourier transforms of Eqs. (A2) and (A3) results in differential equations nearly identical to Eqs. (11) and (12) except with $\alpha_1 = 1/\Lambda_1(i\omega C_1 + \eta_1 \Lambda_1 4\pi^2 k^2 + g)$ and $\alpha_2 = 1/\Lambda_2(i\omega C_2 + \eta_2 \Lambda_2 4\pi^2 k^2 + g)$. The temperature profile for any layer in the two-channel multilayer will have the same form as Eq. (13).

In standard TDTR experiments, the surface layer is a metal film that serves as a transducer. The pump beam heats the metal's electrons, while the probe beam primarily interrogates the temperature of the metal's phonons.[31] Assigning electrons to channel 1 and phonons to channel 2 yields

$$G(k) = \frac{u_1 B_1^- + u_2 B_2^- + u_1 B_1^+ + u_2 B_2^+}{\gamma_{11} v_1 B_1^- + \gamma_{12} v_2 B_2^- - \gamma_{11} v_1 B_1^+ - \gamma_{12} v_2 B_2^+}, \tag{A4}$$

where $\gamma_{mn} = \Lambda_m \lambda_n$.

To solve for the surface temperature of a layer in terms of the surface heat flux, it is necessary to relate the temperature profiles and heat currents between layers. This can be accomplished by applying thermal boundary conditions to each layer and requiring conservation of energy across boundaries and then solving the resulting system of equations. We generalize this approach for an arbitrary number of layers by deriving an iterative expression, analogous to Eq. (14) in Ref. 22, which relates the unknown constants in Eq. (13), $[B] = (B_1^- \;\; B_2^- \;\; B_1^+ \;\; B_2^+)^T$ to the values for $[B]$ of the layer beneath it. To do this we need a matrix that relates a layer's values of $[B]$ to the temperatures and heat fluxes at the bottom of that layer, a matrix that relates the temperatures and heat fluxes of two layers at a boundary, and a matrix that relates the surface temperature and heat fluxes of a layer to its values of $[B]$.

The values of $[B]$ can be expressed in terms of the temperatures and heat fluxes at the bottom of that layer with the expression

$$[B] = [M][T_1 \quad T_2 \quad q_1 \quad q_2]_{z=L}^T, \tag{A5}$$

$$[M] = \frac{1}{2} \begin{bmatrix} e^{\lambda_1 L} & 0 & 0 & 0 \\ 0 & e^{\lambda_2 L} & 0 & 0 \\ 0 & 0 & e^{-\lambda_1 L} & 0 \\ 0 & 0 & 0 & e^{-\lambda_2 L} \end{bmatrix} \begin{bmatrix} [X]^{-1} & [Y]^{-1} \\ [X]^{-1} & -[Y]^{-1} \end{bmatrix}, \tag{A6}$$

where L is the layer thickness and $[X]$ and $[Y]$ are defined in Eqs. (14) and (16). The temperatures and heat fluxes at a

surface of a two-channel layer can be expressed as

$$(T_1 \quad T_2 \quad q_1 \quad q_2)^T_{z=0} = [N][B], \tag{A7}$$

$$[N] = \begin{bmatrix} [X] & [X] \\ [Y] & -[Y] \end{bmatrix}. \tag{A8}$$

Heat flow between layers at an interface can be described using four interface conductance values, G_{11}, G_{12}, G_{21}, G_{22}, where the subscripts denote the channels between which G describes heat flow. Consider as an example the Al/$Si_{0.099}Ge_{0.01}$ system with low- (<3 THz) and high-frequency phonons grouped into channels 1 and 2. Then the G_{11} and G_{22} terms are related to the strength of coupling between the low- and high-frequency phonon reservoirs in the two layers. The terms G_{12} and G_{21} relate the coupling of low-frequency Al phonons to high-frequency Si phonons and high-frequency Al phonons to low-frequency Si phonons. These terms will not be equal because selection rules that govern the probability of a three-phonon scattering event will be different for the two cases. In most systems, only one or two of these four conductance values will be needed in the calculation because coupling between different types of carriers across an interface is often weak.

The temperatures and heat fluxes at the bottom of layer n can be related to temperatures and heat fluxes at the surface of layer $n + 1$ with the four interface conductance values

$$[T_1 \quad T_2 \quad q_1 \quad q_2]^T_{n,z=d} = [R][T_1 \quad T_2 \quad q_1 \quad q_2]^T_{n+1,z=0}, \tag{A9}$$

$$[R] = \frac{1}{G_{11}G_{22} - G_{12}G_{21}} \times \begin{bmatrix} CG_{22} & -DG_{21} & G_{22} & -G_{21} \\ -CG_{12} & DG_{11} & -G_{12} & G_{11} \\ \beta & -\beta & EG_{22} & -EG_{21} \\ -\beta & \beta & -FG_{12} & FG_{11} \end{bmatrix}, \tag{A10}$$

$$C \equiv G_{11} + G_{21}, \tag{A11}$$

$$D \equiv G_{12} + G_{22}, \tag{A12}$$

$$E \equiv G_{11} + G_{12}, \tag{A13}$$

$$F \equiv G_{22} + G_{21}, \tag{A14}$$

$$\beta \equiv EG_{22}G_{21} + FG_{11}G_{12}. \tag{A15}$$

Using Eqs. (A.5), (A.7), and (A.9), we can write an iterative expression for the constant matrix $[B]$:

$$[B]_n = [M][R][N][B]_{n+1}. \tag{A16}$$

For analysis of experiments in which the metal transducer is not on the surface of the multilayer stack, meaning heat is deposited and temperature is interrogated at a buried interface in the multilayer system, it is necessary to modify the above solution for $G(k)$ to account for bidirectional heat flow from the transducer. In a bidirectional model, the multilayered system can be split into two stacks: a forward stack consisting of all layers above the boundary where heat is deposited, and a backward stack that includes all layers below. The correct substitution for Eq. (A.4) can be derived by (a) noting energy conservation at the heated boundary, $q_s = q_f + q_b$, where q_f is the heat flow into the forward stack, and q_b is heat flow into the backward stack; and (b) solving the system of equations that results from the separate application of Eq. (A.16) to the forward and backward stack.

Often a single channel is sufficient to describe heat flow in a majority of the system's layers, and the formulation described by Eqs. (A5)–(A16) is computationally wasteful. A more computationally efficient but less general approach is to derive $G(k)$ for a hybrid multilayer, where some layers have two channels and some have one channel. This expression is easily derived for the specific case of a one-channel multilayer on top of a semi-infinite two-channel layer. Applying interfacial conductance heat flux boundary condition to the two-channel layer [Eq. (5)] and substituting Eq. (13) into Eq. (15) yields a system of equations that defines the B_i^- in terms of the bottom of the single-channel layer, T_{SC}:

$$[h]T_{SC} = ([Y] + [h][X])[B^-], \tag{A17}$$

where $[h]$ is a diagonal matrix that contains each channel's interface conductance. By requiring conservation of energy at the surface of the semi-infinite two-channel layer, the total heat flux at the bottom of the single-channel multilayer can be expressed as

$$q_{SC} = \sum_i q_i = \sum_j \sum_i Y_{ij} B_j^- = \Phi T_{SC}. \tag{A18}$$

In standard TDTR analysis, the heat flux at the surface of the semi-infinite substrate is proportionally related to its surface temperature, $q_n = \Lambda_n u_n T_n$, where $u_n = (4\pi^2 k^2 + i\omega C_n/\Lambda_n)$. The major change in analysis when replacing a one-channel semi-infinite layer with a two-channel semi-infinite layer is that $\Lambda_n u_n$ is replaced by Φ:

$$G(k) = \frac{D^+ - \Phi B^+}{\Phi A^+ - C^+}, \tag{A19}$$

where A^+, B^+, C^+, and D^+ are defined in Eq. (A14) in Ref. 28. We note that the B^+ term here is not related to the B terms defined in Eq. (13). A second difference is that for the two-channel semi-infinite substrate case the interfacial conductance values are used to calculate Φ, while for the case of a one-channel substrate the interface conductance is included in the calculation of A^+, B^+, C^+, and D^+. This difference arises because the B^- terms in Eq. (13) for the semi-infinite two-channel layer depend on how the heat flux into the layer is distributed between the channels [Eq. (15)] and can't be assumed to equal 1 as in Ref. 22 for single channel layers.

APPENDIX B: (N + 1) TEMPERATURE MODEL

Electron-electron scattering times are typically much faster than the electron-phonon relaxation time; therefore, the assumption that the electron and phonon channels are well described by a single temperature is often rigorously valid.[10] The same is not true for the low-frequency/high-frequency channels in a phonon system. We do not expect a single temperature to describe the occupation statistics of all low-frequency phonons because scattering rates between low-frequency

acoustic phonons are small, the coupling constant between high- and low-frequency phonons is frequency dependent, and the interface conductance integrand is frequency dependent. To correct this oversimplification, we generalize our approach to allow the low-frequency channel to have N temperatures. To limit the number of additional thermal property parameters in the model, we follow Ref. 21 and assume that coupling between low-frequency phonons is negligible. Then, the two coupled differential equations in Eq. (11) and Eq. (12) become a system of $N + 1$ coupled differential equations:

$$\begin{aligned}\frac{\partial^2 T_0}{\partial z^2} &= \alpha_0 T_0 - \sum_n \frac{g_n}{\Lambda_0} T_n \\ \frac{\partial^2 T_1}{\partial z^2} &= \alpha_1 T_1 - \frac{g_1}{\Lambda_1} T_0 \\ &\vdots \\ \frac{\partial^2 T_N}{\partial z^2} &= \alpha_N T_N - \frac{g_N}{\Lambda_N} T_0,\end{aligned} \tag{B1}$$

where $\alpha_0 = 1/\Lambda_0(i\omega C_0 + G_R)$, $\alpha_n = 1/\Lambda_n(i\omega C_n + g_n)$, $G_R = \sum_n g_n$, T_0 is the temperature of the high-frequency phonon thermal reservoir, and T_1 to T_N describe the N low-frequency channels. The value of G_R quantifies the rate of energy transfer from the high-frequency channel by radiation and absorption of low-frequency phonons.[21] The temperature profiles in B1 can be found in an identical manner to T_1 and T_2 in Eqs. (11) and (12). The only change is that the matrices in Eqs. (13)–(16) will have a rank of $N + 1$ instead of 2.

The characteristic polynomial for the eigenvalues is

$$(\alpha_0 - \lambda^2)\prod_{n=1}^{N}(\alpha_n - \lambda^2) - \sum_{n=1}^{N}\left(\frac{g_n^2}{\Lambda_0\Lambda_n}\frac{1}{(\alpha_n - \lambda^2)}\prod_{n=1}^{N}(\alpha_n - \lambda^2)\right) = 0. \tag{B2}$$

In the steady-state limit, $\alpha_n = g_n/\Lambda_n$, and the length scale of nonequilibrium between channels is given by $1/\lambda$. Considering Eq. (B2), we see that the range of length scales describing nonequilibrium will be of order $\sqrt{\Lambda_0/G_R}$ to $\sqrt{\Lambda_M/g_M}$, where M labels the channel with weakest coupling to the high-frequency thermal reservoir.

In order to use an $(N + 1)$ temperature model to generate TDTR data, it is necessary to define $(N + 1)$ interface conductance values, thermal conductivities, heat capacities, and coupling parameters. To reduce the number of free parameters, we need frequency-dependent expressions for these properties. For example, let channel i contain phonons with frequency ω to $\omega + \Delta\omega$. Then its thermal conductivity can be approximated as $\Lambda_i = (C(\omega)v^2\tau(\omega)/3)\Delta\omega$. The phonon-phonon scattering rate for low-frequency phonons can be approximated as $\tau(\omega)^{-1} = B_S\omega^2$, where B_S is the scattering strength. The low-frequency heat capacity can be approximated as $C(\omega) = 3k_B\omega^2/(2v^3\pi^2)$. Assuming that the low-frequency scattering time is equal to the thermal relaxation time between high- and low-frequency phonons allows the coupling constant of channel i to be approximated as $g_i = C(\omega)\Delta\omega/\tau(\omega) = 3k_B B_S\omega^4\Delta\omega/(2v^3\pi^2)$. Similarly, we can approximate the interface conductance of channel i as $G_i = v(1 - R)C(\omega)\Delta\omega/4$. Now the thermal parameters in the model are R, B_S, v, Λ_{Tot}, C_{Tot}, and G_{Tot}. For $Si_{0.99}Ge_{0.01}$, values of $B_S = 6.5 \times 10^{-17}$s, $\Lambda_{Tot} = 44\ W\ m^{-1}K^{-1}$, and $G_{Tot} = 260\ MW\ m^{-2}\ K^{-1}$, $R = 0$, $v = 6000$ m/s, and $C_{Tot} = 1.65\ J\ cm^{-3}$ result in excellent agreement between the $(N + 1)$ temperature model and experiment for $N = 20$. In this calculation, we included only phonons with frequencies between 0.5 THz and 3 THz in the low-frequency channel and assumed modes with a frequency less than 0.5 THz do not carry heat because of Akhiezer damping.[32] We note that the value we derive for B_S depends on the value we assumed for R. A value of $B_S = 6.5 \times 10^{-17}$s corresponds to $G_R = 3 \times 10^{14}\ W\ m^{-1}\ K^{-1}$, comparable to the value of $g = 4 \times 10^{14}\ W\ m^{-1}\ K^{-1}$ derived using the two-channel model.

*Corresponding author: wilson81@illinois.edu

[1] A. Majumdar and P. Reddy, Appl. Phys. Lett. **84**, 4768 (2004).
[2] M. Highland, B. C. Gundrum, Y. K. Koh, R. S. Averback, D. G. Cahill, V. C. Elarde, J. J. Coleman, D. A. Walko, and E. C. Landahl, Phys. Rev. B **76**, 075337 (2007).
[3] Y. K. Koh and D. G. Cahill, Phys. Rev. B **76**, 075207 (2007).
[4] J. A. Johnson, A. A. Maznev, J. Cuffe, J. K. Eliason, A. J. Minnich, T. Kehoe, Clivia M. Sotomayor Torres, G. Chen, and K. A. Nelson, Phys. Rev. Lett. **110**, 025901 (2013).
[5] A. J. Minnich, J. A. Johnson, A. J. Schmidt, K. Esfarjani, M. S. Dresselhaus, K. A. Nelson, and G. Chen, Phys. Rev. Lett. **107**, 095901 (2011).
[6] K. T. Regner, D. P. Sellan, S. Zonghui, C. H. Amon, A. J. H. McGaughey, and J. A. Malen, Nat. Commun. **4**, 1640 (2013).
[7] W. Wang and D. G. Cahill, Phys. Rev. Lett. **109**, 175503 (2012).
[8] G. D. Mahan and F. Claro, Phys. Rev. B **38**, 1963 (1988).
[9] M. C. Langner, C. L. S. Kantner, Y. H. Chu, L. M. Martin, P. Yu, R. Ramesh, and J. Orenstein, Phys. Rev. B **82**, 054425 (2010).
[10] G. Tas and H. J. Maris, Phys. Rev. B **49**, 15046 (1994).
[11] S. D. Brorson, A. Kazeroonian, J. S. Moodera, D. W. Face, T. K. Cheng, E. P. Ippen, M. S. Dresselhaus, and G. Dresselhaus, Phys. Rev. Lett. **64**, 2172 (1990).
[12] P. B. Allen, Phys. Rev. Lett. **59**, 1460 (1987).
[13] O. M. Wilson, X. Hu, D. G. Cahill, and P. V. Braun, Phys. Rev. B **66**, 224301 (2002).
[14] R. J. Stoner and H. J. Maris, Phys. Rev. B **48**, 16373 (1993).
[15] H.-K. Lyeo and D. G. Cahill, Phys. Rev. B **73**, 144301 (2006).
[16] J. A. Birch, W. R. G. Kemp, P. G. Klemens, and R. J. Tainsh, Aus. J. Phys. **12**, 455 (1959).
[17] W. R. G. Kemp, P. G. Klemens, and R. J. Tainsh, Phil. Magazine **4**, 845 (1959).
[18] G. K. White, S. B. Woods, and M. T. Elford, Phil. Magazine **4**, 688 (1959).
[19] Z. Lin, L. V. Zhigilei, and V. Celli, Phys. Rev. B **77**, 075133 (2008).

[20] A. Ward and D. A. Broido, Phys. Rev. B **81**, 085205 (2010).
[21] A. A. Maznev, J. A. Johnson, and K. A. Nelson, Phys. Rev. B **84**, 195206 (2011).
[22] D. G. Cahill, Rev. Sci. Instrum. **75**, 5119 (2004).
[23] A. D. Zdetsis and C. S. Wang, Phys. Rev. B **19**, 2999 (1979).
[24] A. V. Sologubenko, K. Giannó, H. R. Ott, U. Ammerahl, and A. Revcolevschi, Phys. Rev. Lett. **84**, 2714 (2000).
[25] D. A. Young and H. J. Maris, Phys. Rev. B **40**, 3685 (1989).
[26] B. C. Gundrum, D. G. Cahill, and R. S. Averback, Phys. Rev. B **72**, 245426 (2005).
[27] D. G. Cahill, F. Watanabe, A. Rockett, and C. B. Vining, Phys. Rev. B **71**, 235202 (2005).
[28] J. Liu, J. Zhu, M. Tian, X. Gu, A. Schmidt, and R. Yang, Rev. Sci. Instrum. **84**, 034902 (2013).
[29] C. A. da Cruz, W. Li, N. A. Katcho, and N. Mingo, Appl. Phys. Lett. **101**, 083108 (2012).
[30] J. P. Feser and D. G. Cahill, Rev. Sci. Instrum. **83**, 104901 (2012).
[31] R. B. Wilson, B. A. Apgar, L. W. Martin, and D. G. Cahill, Opt. Express **20**, 28829 (2012).
[32] B. C. Daly, K. Kang, Y. Wang, and D. G. Cahill, Phys. Rev. B **80**, 174112 (2009).